

1 **Photochemical Formation of Trifluoroacetic Acid: Mechanistic**
2 **Insights into a Fluoxetine-Related Aryl-CF₃ Compound**

3

4 Zhefei Guo¹, Azka A. Attar¹, Qiqige Qiqige¹, Rylan J. Lundgren¹, Shira Joudan^{1*}

5

6 ¹Department of Chemistry, University of Alberta, Edmonton T6G 2G2, Alberta, Canada

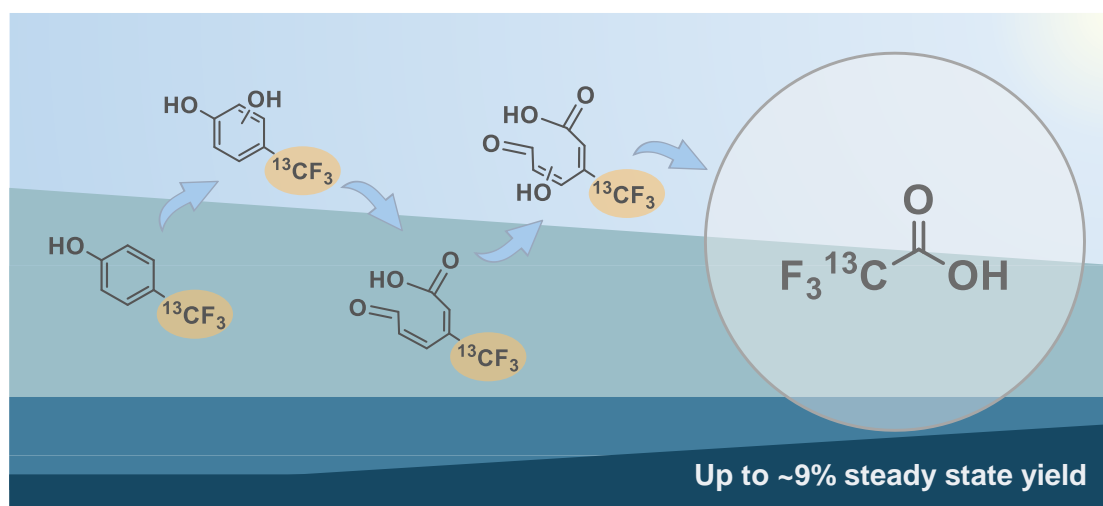
7

8 Email: joudan@ualberta.ca

9

10

11 TOC Art



12

13 ABSTRACT

14 Trifluoroacetic acid (TFA) is a ubiquitous environmental contaminant; however, its sources are
15 poorly constrained. One understudied source is from the photochemical reactions of aromatic
16 compounds containing $-\text{CF}_3$ moieties (aryl- CF_3) including many pharmaceuticals and
17 agrochemicals. Here, we studied the aqueous photochemistry of 4-(trifluoromethyl)phenol (4-
18 TFMP), a known transformation product of the pharmaceutical fluoxetine. When exposed to
19 lamps centred at UV-B, 4-TFMP formed up to 9.2% TFA at steady state under acidic conditions
20 and 1.3% under alkaline conditions. TFA yields of fluoxetine were similar to 4-TFMP for acidic
21 and neutral pH, but higher at alkaline pH, suggesting fluoxetine may have a mechanism of TFA
22 formation in addition to via the 4-TFMP intermediate. Use of a $^{13}\text{CF}_3$ isotopologue of 4-TFMP
23 allowed for the tracking of TFA formation, which formed via multiple oxidative additions prior
24 to oxidative ring cleavage. The oxidation is mediated by reactive oxygen species (ROS)
25 generated through self-sensitized photolysis, with singlet oxygen and hydroxyl radicals as the
26 key ROS. In addition to the TFA formation mechanism, other photochemical reactions of 4-
27 TFMP resulted in defluorination and dimerization. Overall, this work expands the

28 understanding of how TFA forms from aryl-CF₃ compounds to better understand the total global
29 burden of TFA.

30

31 **Synopsis:** 4-(Trifluoromethyl)phenol, a transformation product of fluoxetine, forms up to 9.2%
32 TFA from photolysis via oxidative cleavage of the aromatic ring.

33

34 **Keywords:** Fluoxetine, trifluoroacetic acid, PFAS, aqueous photochemistry, oxidative cleavage,
35 isotope tracking, self-sensitized photolysis, reactive oxygen species

36 INTRODUCTION

37 Trifluoroacetic acid (TFA) is a very persistent and very mobile pollutant ubiquitously present
38 in the environment.¹⁻⁷ TFA is the smallest analogue of perfluoroalkyl carboxylic acids, and
39 according to the OECD definition, is classified as a per- and polyfluoroalkyl substance
40 (PFAS).^{8,9} Reported TFA concentrations in environmental matrices are often higher than other
41 PFAS,^{3,4,7} with rapid increases observed since the 1990s.^{2,5,6,10} This raises concerns about its
42 accumulation in ecosystems and potential human exposure. Although TFA is less
43 bioaccumulative in mammals compared to longer-chain PFAS, it can be uptaken and
44 accumulated by plants.^{11,12} Due to its hydrophilic and mobile nature, TFA is challenging to
45 remove from water, allowing it to migrate into drinking water supplies.^{13,14} In 2016-2017,
46 Scheurer et al. found surprisingly high concentrations of TFA (>100 µg/L) during screening of
47 potable and surface waters in south-west Germany.¹³ Neuwald et al. reported TFA as the most
48 predominant PFAS in German drinking water sources, with a maximum concentration of 12.4
49 µg/L.¹⁵ In an investigation of drinking water in U.S. home, Zheng et al. found that TFA was the
50 predominant PFAS with the median concentration of 79 ng/L and a 95% detection frequency.⁷

51 TFA has many known direct and indirect environmental sources. However, environmental
52 levels of TFA exceed estimations based on both direct emissions of TFA and of known
53 precursors, indicating the existence of uncharacterized sources.¹⁶ A well-identified source of
54 TFA is from atmospheric oxidation of fluorinated gases including hydrofluorocarbons and
55 hydrofluoroolefins.^{17,18} Other sources include thermolysis of fluoropolymers and oxidation of
56 some longer-chain PFAS.¹⁹⁻²¹ An additional known and further speculated class of TFA
57 precursors are compounds containing aromatic CF₃ functional groups, referred to as aryl-CF₃.

58 Modern chemistry incorporates fluorine into pharmaceuticals and agrochemicals to
59 enhance their properties and performance.²² Since the 1950s, fluorine has been integrated into
60 these compounds in various forms, including aryl-CF₃.²³ Examples include the antidepressant
61 fluoxetine, the lampricide 3-trifluoromethyl-4-nitrophenol (TFM), and the herbicide
62 oxyfluorfen. These compounds enter the environment from different point and nonpoint sources,
63 such as wastewater treatment plants (WWTPs) when not effectively removed or mineralized,
64 direct emissions (e.g. TFM directly used in the Great Lakes), and agricultural runoff (e.g.
65 herbicides and pesticides). For instance, fluoxetine is not efficiently removed in WWTPs and
66 is detected in surface waters at concentrations ranging from 1 to 100 ng/L.²⁴ Once in the
67 environment, aryl-CF₃ present in sunlit waters may undergo photochemical reactions. Previous
68 research indicates that defluorination of the -CF₃ moiety is a major pathway for the photolysis
69 of aryl-CF₃ (i.e. C-CF₃ to C-COOH).²⁵ However, depending on aqueous pH and substituents
70 on the aromatic ring, TFA can also be formed.²⁶⁻²⁸ Early laboratory studies by Ellis & Mabury
71 showed that TFM can photochemically form TFA and undergo photo-defluorination via two
72 competing pH-dependent pathways: defluorination is always the favored pathway, becoming
73 more dominant at higher pH, while lower pH enhances the formation of TFA.²⁶ TFA formation
74 has also been observed in more recent research on the direct and indirect photolysis of
75 fluoxetine.^{27,29} Despite these efforts, reaction kinetics and TFA yield under different pH
76 conditions and the mechanism of TFA formation are not sufficiently characterized. To the best
77 of our knowledge, except for the early study on the photolysis of TFM,²⁶ no intermediates have
78 been reported nor mechanism proposed for the formation of TFA from any aryl-CF₃, which is
79 expected to include oxidative cleavage of the aromatic ring.

80 To understand the formation of TFA from some aryl-CF₃ compounds, we investigated the
81 aqueous photolysis of a probe aryl-CF₃ compound, 4-(trifluoromethyl)phenol (4-TFMP) under
82 different pH conditions. 4-TFMP was selected because it is a well-known transformation
83 product (TP) of fluoxetine,²⁹⁻³¹ and has long been hypothesized to be the key intermediate in
84 the photochemical formation of TFA, yet the mechanism of TFA formation has not been
85 elucidated.^{27,29} We determined the reaction kinetics and steady state TFA molar yield (TFA_{ss}%),
86 which represents the total potential of the 4-TFMP to release TFA. Furthermore, we aimed to
87 elucidate the mechanism leading to TFA formation by identifying TPs and by characterizing
88 the possible self-sensitized photochemistry.

89 Stable isotope labeling (SIL) uses stable isotopes (e.g. deuterium and carbon-13) to label
90 compounds and track their TPs.³² In high-resolution mass spectrometry (HRMS) analysis,
91 labeled TPs can be easily distinguished by mass spectrometry due to the mass difference
92 introduced. Several groups have investigated the environmental fate or biotransformation of
93 stable isotope-labeled pollutants, such as ¹³C-labeled poly(butylene succinate) and ²H-labeled
94 6PPD and 6PPD-quinone.³³⁻³⁵ Inspired by SIL, an in-house synthesized ¹³CF₃-labeled 4-TFMP
95 (¹³CF₃-4-TFMP) was used to track the ¹³CF₃-TFA (¹³CF₃COOH) formation and to help identify
96 ¹³C-labeled TPs. Since the structure ¹³CF₃-TFA completely retains -¹³CF₃ group, we
97 hypothesized that ¹³CF₃-TFA would be generated during the photolysis of ¹³CF₃-4-TFMP.
98 Furthermore, we proposed that in the pathway from ¹³CF₃-4-TFMP to ¹³CF₃-TFA, key
99 intermediates would retain the entire -¹³CF₃ group.

100

101

102 MATERIALS AND METHODS

103 Chemicals.

104 All chemicals were used as received. Details on chemicals used are described in the Supporting
105 Information (SI). $^{13}\text{CF}_3$ -4-TFMP was synthesized in-house with 99% isotopic purity of the
106 $^{13}\text{CF}_3$ -carbon. In brief, 1,4-dibromobenzene was treated with n-BuLi followed by $^{13}\text{CO}_2$ to
107 introduce the carbon label.³⁶ The corresponding benzoic acid was reacted with
108 fluolead/HF•pyridine³⁷ to prepare $^{13}\text{CF}_3$ -labeled 4-bromobenzotrifluoride. Nucleophilic
109 substitution with benzyl alcohol under basic conditions followed by Pd/C hydrogenolysis
110 yielded $^{13}\text{CF}_3$ -4-TFMP in 24% overall yield over four steps (see SI-2 for full details).

111 Photolysis Experiments.

112 Aqueous stock solutions (5 mM) of 4-TFMP, $^{13}\text{CF}_3$ -4-TFMP, and fluoxetine were prepared in
113 ultrapure water for photolysis experiments. Prior to the experiment, the stock solutions were
114 diluted with 0.5 mM acidic, neutral, or alkaline phosphate buffer to achieve an initial
115 concentration of 50 μM in a 100 mL polypropylene (PP) volumetric flask. $^{13}\text{CF}_3$ -4-TFMP
116 experiments were performed in ultrapure water. The solutions were then transferred into 10 mL
117 quartz tubes. For each experiment, three quartz tubes were kept in the dark as a control, and the
118 other three were placed in the photoreactor. Photolysis experiments were carried out in a
119 Luzchem LZC photoreactor equipped with 14 lamps centered at 311 nm in the UV-B region
120 (Figure S5), distributed on the ceiling and two opposite inner sides of the photoreactor. The
121 quartz tubes were placed on a carousel and rotated at a low speed to ensure that each tube was
122 evenly exposed to the UV-B light. Samples were taken at set intervals for a suite of analysis.

123 To verify the self-sensitized photolysis mechanism of 4-TFMP, experiments using

124 different initial concentrations of 4-TFMP of 4 μM and 85 μM were carried out in ultrapure
125 water. To identify if hydroxyl radicals were formed during photolysis, duplicate photolysis
126 experiments were performed in ultrapure water in the presence of excessive (20 mM and 80
127 mM) methanol.³⁸ To determine if singlet oxygen ($^1\text{O}_2$) was produced, duplicate photolysis
128 experiments were performed in the presence of excessive (20 mM) furfuryl alcohol (FFA)³⁹ and
129 in 99% D_2O .^{40,41}

130 The *para*-nitroanisole (PNA) actinometer was used to evaluate the quantum yield,⁴²
131 following a setup previously described.^{28,43,44} Briefly, PNA was dissolved in acetonitrile as a
132 stock solution, then further diluted in ultrapure water to an initial concentration of 10 μM with
133 0.2% acetonitrile as the co-solvent. Photolysis of PNA were performed in triplicate using the
134 same quartz tubes. The pseudo-first-order rate constant for PNA was determined, and the
135 revised quantum yield of 0.00029 was used to calculate the quantum yield of 4-TFMP (see **eq**
136 **S1** for calculation details).^{45,46}

137 **Analytical Methods.**

138 **High performance liquid chromatography with UV detection (HPLC-UV).** At set sampling
139 events, 200 μL was aliquoted into an autosampler vial with a PP insert for HPLC analysis. A
140 Waters 2695 Alliance HPLC coupled to a Waters 2487 dual-wavelength UV detector was used
141 to quantify 4-TFMP, fluoxetine, PNA, and a transformation product of 4-TFMP, 4-
142 hydroxybenzoic acid (4-HBA). Retention and separation were achieved using a Poroshell EC-
143 C18 column (2.7 μm , 4.6 \times 50 mm) (details in **Table S3**). All standards were prepared from
144 neat material dissolved in methanol.

145 **Ion chromatography (IC).** At set sampling events, 600 μL was aliquoted into a PP vial for IC

146 analysis with conductivity detection. Fluoride (F^-) and TFA were quantified by a Dionex ICS-
147 5000+ equipped with an AS18 analytical column (4×250 mm) and Dionex ADRS 600 4 mm
148 suppressor. Gradient elution with NaOH was used to retain and separate F^- and TFA from
149 matrix anions including the phosphate buffer (details in **Table S4**).

150 **UHPLC-MS/MS.** $^{13}CF_3$ -TFA was quantified from photolysis experiments of $^{13}CF_3$ -4-TFMP.
151 Aliquots were diluted $10\times$ to a final composition of 10% methanol before analysis using a
152 Waters Acquity ultra-high performance liquid chromatography (UHPLC) system coupled to a
153 Waters Xevo TQ-S triple quadrupole mass spectrometer using a Luna Omega PS C18 column
154 ($1.6 \mu m$, 2.1×50 mm) to retain polar TFA. $^{13}CF_3$ -TFA was quantified by external calibration
155 using the commercially available $^{13}CO_2$ -TFA ($CF_3^{13}COOH$) (details in **Table S5**).

156 **UHPLC-Orbitrap-HRMS.** Triplicate samples from 4-TFMP or $^{13}CF_3$ -4-TFMP photolysis
157 were combined as a pooled sample and diluted $10\times$ to a final composition of 10% methanol
158 before analysis. Suspect and non-targeted screening of TPs was performed using a Thermo
159 Vanquish UHPLC coupled to a Thermo Scientific Orbitrap Exploris 240 HRMS and a Luna
160 Omega Polar C18 column ($1.6 \mu m$, 2.1×50 mm). Data were acquired under both positive and
161 negative electrospray ionization mode as separate injections by full scan (m/z range 50–750,
162 resolution 60 000) (details in **Table S6**). Targeted MS^2 (t MS^2) with a suspect list and data-
163 dependent acquisition (DDA) were used to gain structural information (see **SI-11**). Fluoxetine
164 experiments were analyzed to confirm 4-TFMP and its other major TP.

165 **^{19}F NMR.** For the ^{19}F NMR experiments, a higher initial concentration of 100 μM 4-TFMP or
166 fluoxetine in ultrapure water were used due to the ^{19}F NMR sensitivity limitation. At select
167 times, a 540 μL aliquot was placed in an NMR tube and 60 μL D_2O was added. Non-targeted

168 screening of all fluorinated species was conducted on an Agilent 400 MHz NMR (376 MHz for
169 ^{19}F NMR). The scan range was from +30 to -165 ppm to cover organic fluorine and inorganic
170 fluoride, and 1152 scans were obtained to improve the signal-to-noise ratio (details in **Table**
171 **S7**).

172 **Kinetics Modeling.**

173 For 4-TFMP experiments, pseudo-first-order kinetics equations were applied to 4-TFMP
174 degradation, and a parallel reaction kinetics model was used to fit the normalized TFA
175 concentration generated over time, providing the rate constant of TFA formation, and the $\text{TFA}_{\text{ss}}\%$
176 (see **eq S2-eq S7**). For fluoxetine experiments, we focused only on the $\text{TFA}_{\text{ss}}\%$, which was
177 calculated using the software COPASI⁴⁷ for kinetics modelling. Please refer to the **SI-4** for more
178 details.

179

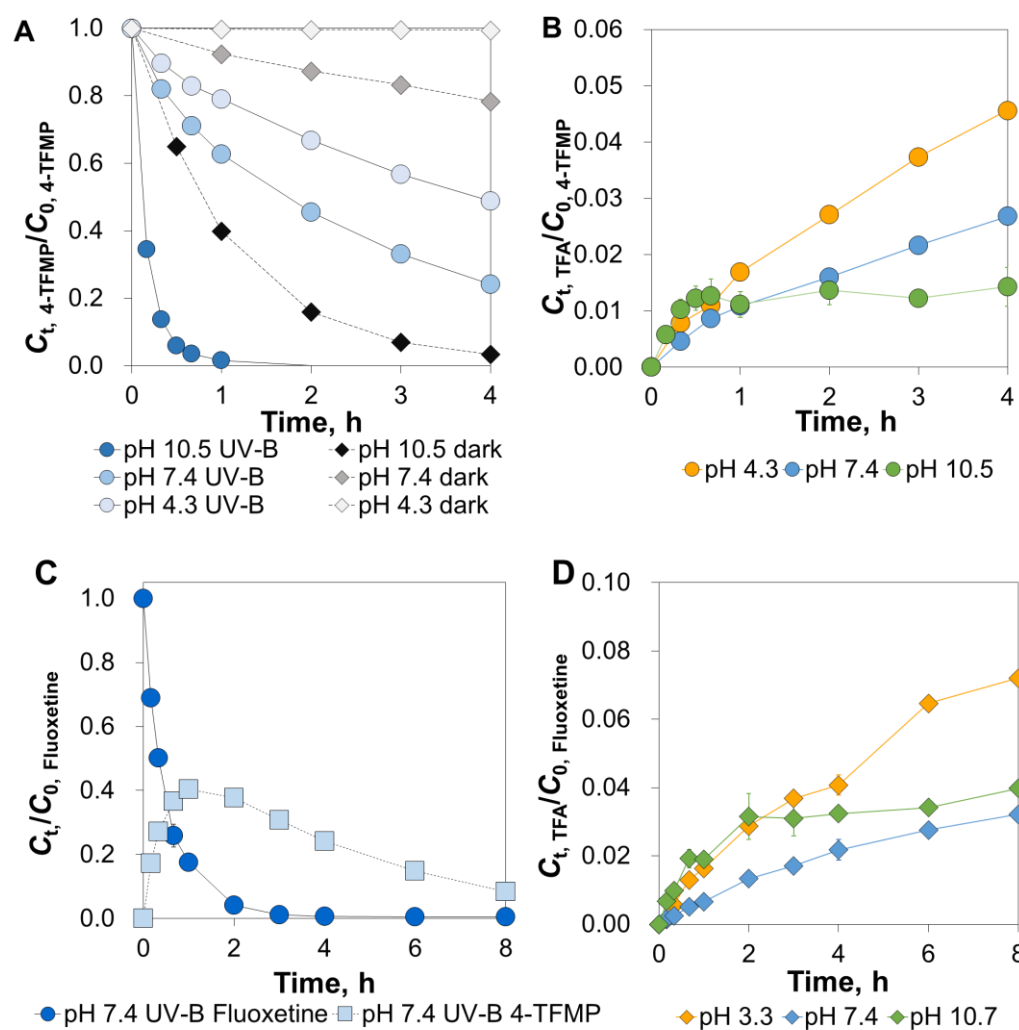
180 **RESULTS AND DISCUSSION**

181 **pH Dependent Photochemical TFA Formation**

182 All 4-TFMP and fluoxetine aqueous photochemistry experiments produced TFA as a product,
183 with pH influencing the yields and rates of TFA formation. **Figure 1A** shows the degradation
184 of 4-TFMP in different pH solutions, with higher pH levels resulting in faster degradation, both
185 in the presence and absence of UV-B light. This observation is consistent with Bhat et al.'s
186 report on the photolysis of 4-TFMP, despite the use of different light sources.²⁷ In dark controls,
187 the pH-dependent degradation of 4-TFMP is attributed to hydrolysis, driven by the
188 deprotonation of the phenol-OH group. The pKa of the phenol-OH in 4-TFMP is 8.1,⁴⁸ thus,
189 under acidic conditions (pH 4.3), the phenol-OH remains protonated, and is less reactive to

190 hydrolysis. Under neutral to alkaline conditions (pH 7.4 to pH 10.5), 4-TFMP exists as either
191 partially (~17%) or fully (>99%) the phenolate, which facilitates the spontaneous degradation
192 and defluorination reaction likely via the E1cB mechanism.⁴⁹ In both pH 7.4 and pH 10.5 dark
193 controls, 4-TFMP underwent defluorination, releasing three equivalents of F⁻ and forming the
194 corresponding benzoic acid, 4-HBA (**Figure S6** and **Figure S7**). For all photochemistry
195 experiments, the defluorination of 4-TFMP was greater than corresponding dark controls at the
196 same pH, confirming that defluorination also occurred due to photochemistry and not solely
197 hydrolysis (**Figure S7**). Due to the high electron density of the phenoxide anion (i.e. the
198 deprotonated 4-TFMP), which can delocalize onto the benzene ring, the UV-Vis absorption
199 spectrum of 4-TFMP exhibits a red shift, resulting in greater overlap with the lamps used in
200 these experiments (**Figure S5**), leading to an increased photolysis rate, a phenomenon that has
201 been discussed.²⁵⁻²⁷ The quantum yield of these direct photochemistry reactions were highest
202 for 4-TFMP at pH 4.3 and lowest at pH 10.5 (**Table 1**). Since the reaction rate constants and
203 quantum yields have inverse trends across the pH range, it seems that the increased absorption
204 due to the red shift of the phenolate drives the faster reactivity at higher pH.

205 **Figure 1B** shows TFA was formed during 4-TFMP photolysis at all three pH levels tested,
206 but the formation kinetics and yield were both impacted by pH. An early study also observed
207 TFA formation across pH levels from TFM, a lampricide structurally similar to 4-TFMP, as
208 both have phenolic-OH and a -CF₃ group.²⁶ However, a recent study on 4-TFMP photolysis
209 did not detect TFA under alkaline conditions (pH 10), likely due to the sensitivity limitations of
210 their quantitative ¹⁹F NMR method.²⁷



211

212 **Figure 1.** Photolysis of 4-TFMP (panels A and B) and fluoxetine (panels C and D) and the formation of

213 TFA: time trend for (A) 4-TFMP photodegradation (including dark control groups); (B) the formation of

214 TFA from 4-TFMP; (C) fluoxetine degradation and the formation/decay of 4-TFMP as an intermediate

215 (only the pH 7.4 is shown here); and (D) the formation of TFA from fluoxetine. Note that concentrations

216 measured throughout experiments were normalized to the initial concentration of 4-TFMP or fluoxetine.

217 Mean and standard deviation of triplicates are shown.

218

219 TFA formation from 4-TFMP photolysis was fastest at pH 10.5 with a rate k_{TFA} of 0.055 h^{-1}

220 ¹, however, as the reaction reached steady state, the $\text{TFA}_{\text{ss}}\%$ was the highest at pH 4.3, with a

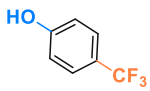
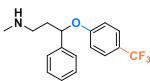
221 predicted molar yield of 9.2% (**Table 1**). This observation emphasizes the need to quantify TFA
222 across multiple time points of the experiments, because the conclusion will be misleading if the
223 measurement of TFA was made early in the reactions. As shown in **Figure 1B**, TFA
224 concentrations from 4-TFMP photolysis were initially higher under alkaline conditions (pH
225 10.5) compared to the other pH levels during the first 40 minutes, but quickly plateaued at a
226 TFA_{ss}% of 1.3% after 40 minutes. These kinetics may be attributed to the rapid hydrolysis
227 reaction occurring under alkaline conditions, which competes with the pathway of TFA
228 formation and quickly degrades 4-TFMP by defluorination. The result that 4-TFMP photolysis
229 under acidic condition generated more TFA aligns with previous research on this compound
230 and the related TFM.^{26,27} The TFA generated was a terminal product and was stable when
231 irradiated with UV-B light (see **Figure S9**).

232 Fluoxetine remained stable in dark control groups buffered across acidic to alkaline pH
233 levels (**Figure S10**), which is consistent with previous research on the laboratory stability test
234 of fluoxetine.⁵⁰ This stability may be attributed to the absence of the acidic hydrogen from the
235 phenol-OH group, which is present in 4-TFMP but not in fluoxetine's structure. **Figure 1C** and
236 **Figure S10** show the photolysis of fluoxetine at different pH levels, where 4-TFMP was an
237 intermediate that was generated and then degraded away, which has been previously
238 observed.^{27,29,30} Our UHPLC-HRMS results identified α -[2-(methylamino)ethyl]benzyl alcohol
239 as the TP of the other half of fluoxetine during cleavage of the alkyl aryl ether bond (**Table S9**).
240 Under alkaline conditions (pH 10.7), 4-TFMP concentration remained relatively low, likely due
241 to its rapid photolysis and hydrolysis after formation. **Figure 1D** shows the formation of TFA
242 during fluoxetine photolysis across various pH levels. The TFA_{ss}% from fluoxetine predicted

243 by the kinetic model was 8.0% and 3.8% under acidic and neutral conditions, respectively,
 244 comparable to that of 4-TFMP under acidic and neutral conditions. Similar to 4-TFMP
 245 photolysis, fluoxetine produced TFA the fastest under alkaline conditions but the most TFA
 246 under acidic conditions. However, under alkaline conditions, TFA_{ss}% from fluoxetine
 247 photolysis was 3.4% compared to only 1.3% from 4-TFMP photolysis (**Table 1**). Contrary to
 248 previous studies that suggest 4-TFMP as the only relevant -CF₃ species for TFA formation,^{27,29}
 249 our findings indicate that fluoxetine may generate TFA through an additional intermediate that
 250 does not involve 4-TFMP. Future work should investigate the formation of TFA from fluoxetine
 251 directly, or through a pathway involving an intermediate other than 4-TFMP.

252

253 **Table 1.** Summary table of 4-TFMP hydrolysis rate constant ($k_{\text{hydrolysis}}$), 4-TFMP photolysis rate constant
 254 ($k_{\text{photolysis}}$), 4-TFMP photolysis quantum yields (Φ), TFA formation rate constant (k_{TFA}), and steady-state
 255 TFA molar yield (TFA_{ss}%) from 4-TFMP or fluoxetine photolysis. Note that photolysis rate constants are
 256 corrected for dark reactions (i.e. hydrolysis).

Compound	pH	4.3	7.4	10.5
 4-TFMP	$k_{\text{hydrolysis}}$ (h ⁻¹)	-	0.059 ± 0.003	0.86 ± 0.01
	$k_{\text{photolysis}}$ (h ⁻¹)	0.173 ± 0.004	0.284 ± 0.008	3.3 ± 0.2
	Quantum yield (Φ)	0.147 ± 0.004	(7.0 ± 0.2) × 10 ⁻³	(3.6 ± 0.2) × 10 ⁻³
	k_{TFA} (h ⁻¹)	(1.6 ± 0.02) × 10 ⁻²	(1.2 ± 0.02) × 10 ⁻²	(5.5 ± 0.2) × 10 ⁻²
	TFA _{ss} %	(9.2 ± 0.2) %	(3.5 ± 0.1) %	(1.3 ± 0.3) %
Compound	pH	3.3	7.4	10.7
 Fluoxetine	TFA _{ss} %	8.0%	3.8%	3.4%

257

258

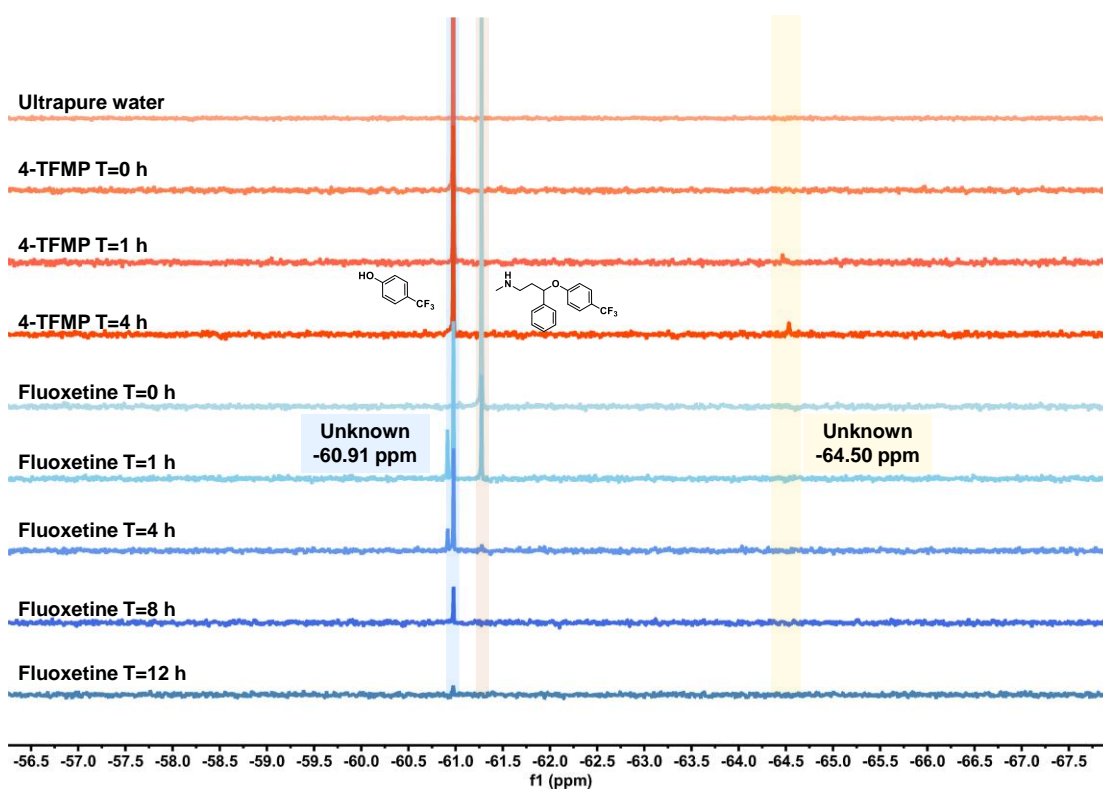
259

260 Identification of Additional Transformation Products

261 The fluorine mass balance of 4-TFMP in dark control and photolysis experiments at different
262 pH were between 80%-120% based on targeted analysis of 4-TFMP, TFA and F⁻ (**Figure S7**),
263 suggesting that the major fluorinated products had were quantified. Since TFA and F⁻ are both
264 terminal products, any missing fluorine must be from intermediates that form and then react
265 away during the experiments, due to either photolysis or hydrolysis. These intermediates will
266 be discussed below based on ¹⁹F NMR and HRMS results and proposed mechanistic
267 intermediates. Targeted analysis of the defluorination product 4-HBA, which contains no
268 fluorine atoms, showed distinct differences between dark controls and photolysis experiments
269 (**Figure S6**). In the dark controls, 4-TFMP hydrolyzed to produce 4-HBA, with its
270 concentration gradually increasing. On the other hand, in the photolysis experiments, although
271 the defluorination rate was higher than in the corresponding dark controls, the concentrations
272 of 4-HBA were lower, which suggests other defluorination pathways may exist, or that 4-TFMP
273 underwent photochemical reactions itself. The time trend of 4-HBA concentrations in
274 photochemistry experiments suggests it formed and then reacted away. The fluorine mass
275 balance for fluoxetine photolysis was lower than that of 4-TFMP, especially at acidic pH based
276 on quantification of fluoxetine, 4-TFMP, TFA and F⁻, suggesting the existence of more
277 fluorinated intermediates (**Figure S7**).

278 Non-targeted screening of fluorinated TPs was conducted using ¹⁹F NMR. ¹⁹F NMR offers
279 significant advantages over other analytical techniques, such as mass spectrometry, in
280 characterizing the environmental fate of fluorochemicals because it is not depended on
281 physicochemical properties of the molecules, only that they contain F-atoms.^{28,51} The natural

282 fluorine nuclei is 100% abundant in ^{19}F and is NMR-active, and fluorine's wide spectral
283 window minimizes peak overlap between structurally similar fluorine atoms. Additionally, the
284 lack of naturally occurring organofluorine compounds enhances the confidence in identifying
285 peaks in the spectrum.^{52,53}



286

287 **Figure 2.** ^{19}F NMR spectra of blank (ultrapure water), 4-TFMP photolysis samples (starting with 100
288 μM in ultrapure water) taken at 0, 1, and 4 hours, and fluoxetine photolysis samples (starting with 100
289 μM in ultrapure water) taken at 0, 1, 4, 8, and 12 hours. Chemical shifts (ppm) from left to right: -60.91
290 (an unknown TP in fluoxetine photolysis), -60.98 (4-TFMP), -61.27 (fluoxetine), -64.50 (an unknown
291 TP in 4-TFMP photolysis). TFA formed from precursors was confirmed at -75.40 ppm, and F^- at -125
292 ppm (Figure S8).

293

294 **Figure 2** shows the ^{19}F NMR spectra of 4-TFMP and fluoxetine photolysis samples
295 collected over time. A growing peak at -64.50 ppm indicates the formation of an unknown

296 fluorinated molecule during 4-TFMP photolysis. Bhat et al. observed a similar peak in the direct
297 photolysis of 4-TFMP in acetate buffer, with no structure assigned.²⁷ As this resonance lies
298 within the $-CF_3$ region and between the 4-TFMP- CF_3 and TFA- CF_3 resonances, it may
299 represent an intermediate leading to the formation of TFA from 4-TFMP. ^{19}F NMR spectra from
300 fluoxetine photolysis experiments confirmed the formation and decay of 4-TFMP (-60.98 ppm).
301 However, the -64.50 ppm peak present in 4-TFMP photolysis was not observed in fluoxetine
302 photolysis. Instead, a new peak appeared at -60.91 ppm, which exhibited an increase, then
303 decrease trend characteristic of a reaction intermediate. This species may account for some of
304 the missing fluorine mass balance during fluoxetine photolysis. Overall, the fluorine mass
305 balance for the aqueous photochemistry of fluoxetine decreased, then increased over the course
306 of the reaction (**Figure S7**), complementary to the trend the peak at -60.91 ppm, suggesting it
307 acts as a reaction intermediate before conversion to TFA or F^- . In a previous study on the
308 photolysis of fluoxetine at a lower concentration and in a different buffer, no new peaks were
309 observed to the left (i.e. downfield) of the intermediate 4-TFMP peak in ^{19}F NMR spectra.²⁷
310 However, in those experiments, NMR spectra were only obtained at the beginning and end of
311 the reaction, so the intermediates may have been missed. Norfluoxetine is a well-characterized
312 metabolite and photolysis product of fluoxetine;^{29,31,54,55} however, comparing with a
313 norfluoxetine standard, no evidence of its formation was supported in either ^{19}F NMR
314 (norfluoxetine -61.31 ppm) or HRMS.

315

316

317

318 Mechanistic Insights into TFA Formation

319 The introduction of the ^{13}C isotope did not affect the photolysis rate of 4-TFMP, nor steady state
320 yield of TFA (~9%) (**Figure S11**). A main advantage to having the $^{13}\text{CF}_3$ label for TFA
321 specifically is that there is no concern about laboratory contamination (e.g. from plastic tubing⁵⁶
322 or as a mobile phase additive). We can be certain the $^{13}\text{CF}_3$ -TFA observed is formed as a product
323 of $^{13}\text{CF}_3$ -4-TFMP and not a potential impurity by monitoring specifically for this isotopologue
324 using targeted triple quadrupole mass spectrometry (**Table S5**).

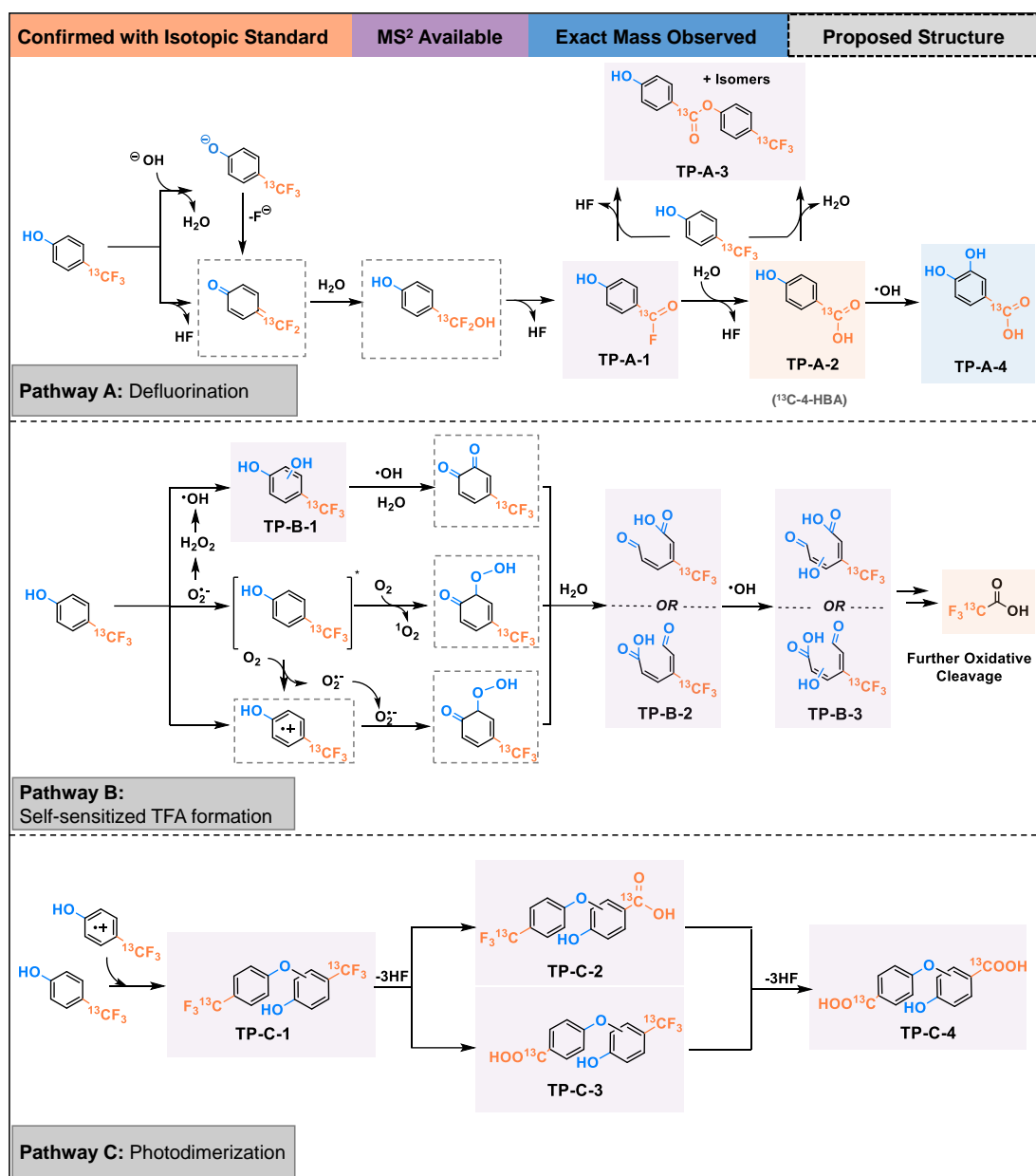
325 **Figure 3** is drawn using $^{13}\text{CF}_3$ -4-TFMP and its TPs and shows the photolysis of 4-TFMP
326 was divided into three distinct pathways: A) defluorination; B) self-sensitized TFA formation;
327 C) photodimerization. These findings highlight the complexity of the 4-TFMP photolysis
328 reactions. Confirmed and proposed intermediates were drawn based on combining Orbitrap
329 HRMS full scan, tMS², and DDA analysis. These TPs were identified with different levels of
330 confidence and are summarized in **Table S8**. Unlabeled and $^{13}\text{CF}_3$ -labeled substances were
331 compared in the same table, with MS² spectra provided in **Figure S12**.

332 *Pathway A, defluorination:* Defluorination is initiated either spontaneously in the dark in
333 higher pH buffers via reaction at the phenolate or through HF elimination under UV-B
334 photolysis. The presumed intermediate is a difluoromethylene quinone, however, similar to
335 other researchers, we were unable to observe it using ^{19}F NMR and HRMS, likely due to its
336 short lifetime in aqueous solution as a highly reactive conjugated electrophile.²⁹ Subsequently,
337 this proposed electrophilic species undergoes nucleophilic addition with water to form a
338 $^{-13}\text{CF}_2\text{OH}$ structure, which then eliminates HF. Previous studies on PFAS degradation have
339 noted that in aqueous solutions, this $^{-13}\text{CF}_2\text{OH}$ group can easily eliminate HF, forming a acyl

340 fluoride.²⁰ The benzoyl fluoride intermediate TP-A-1 was detected by HRMS but its
341 characteristic acyl fluoride resonance was not observed by ¹⁹F NMR. A study on the photo-
342 defluorination of *N,N*-dimethyl-3-(trifluoromethyl)aniline in water and acetonitrile
343 successfully isolated and identified the corresponding benzoyl fluoride intermediate.⁵⁷

344 TP-A-1 further reacts with water to produce the hydrolysis product TP-A-2 (¹³C-4-HBA),
345 which was a major product in the dark controls. Unexpectedly, TP-A-1 also reacts with ¹³CF₃-
346 4-TFMP to form a ¹³C-labeled trifluoromethylated hydroxybenzoate, TP-A-3, in both dark
347 controls and UV-B photolysis. The rapid formation of TP-A-2 from ¹³CF₃-4-TFMP, quickly
348 followed by its conversion to TP-A-3, may explain why the fluorine mass balance of 4-TFMP
349 at pH 10.5 deviated from 100% at the beginning of the reaction and remained relatively constant
350 thereafter (**Figure S7**). Under UV-B photolysis, the extracted ion chromatograms (EIC) from
351 the HRMS for the same *m/z* as TP-A-3 showed multiple chromatographically separated peaks
352 (**Table S8**), suggesting the formation of isomers during the photolysis. The further conversion
353 of TP-A-2 into other TPs upon UV-B is consistent with the quantitative analysis of 4-HBA.
354 Phenol (*m/z* of [M-H]⁻ = 93.0346) was identified as an in-source fragment of 4-HBA rather
355 than a TP, and therefore, 4-HBA does not decarboxylate under UV-B irradiation.

356



357

358 **Figure 3.** Proposed pathways for ¹³CF₃-4-TFMP photolysis. Note that for dimerization products and

359 some hydroxylation products, we were unable to determine the exact substitution positions.

360

361 *Pathway B, self-sensitized TFA formation:* A series of ¹³CF₃-4-TFMP-oxygen addition TPs

362 were detected by HRMS, including ¹³CF₃-4-TFMP+O (TP-B-1), +2O (TP-B-2), and +3O (TP-

363 B-3). ¹³CF₃-4-TFMP+O was identified as a hydroxylation product because it had a similar

364 chromatographic retention time to ¹³CF₃-4-TFMP (**Table S8**) and had HF-eliminated fragments

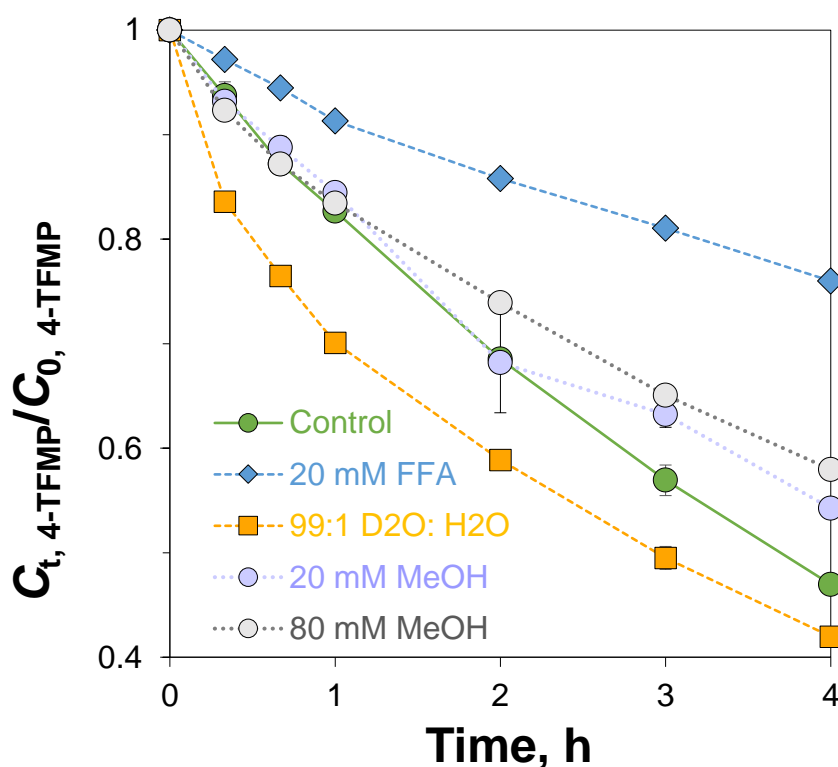
365 in its MS² spectrum that preserve the benzene ring (**Figure S12C**). ¹³CF₃-4-TFMP+O was
366 observed as two chromatographically separated EIC peaks, suggesting the ·OH radicals oxidize
367 non-selectively at both the *ortho* and *meta* positions relative to the -¹³CF₃ group. Interestingly,
368 ·OH radicals were also captured by ¹³C-4-HBA, the hydrolysis defluorination product. ¹³C-4-
369 HBA is a ·OH radical probe, and previous studies have shown that its reaction with ·OH
370 produces a single product, 3,4-dihydroxybenzoic acid, which was detected by HRMS as TP-A-
371 4.^{58,59} TP-B-1 can be further oxidized to TP-B-2 and subsequently to TP-B-3. Both TP-B-2 and
372 TP-B-3 had much earlier retention times compared to ¹³CF₃-4-TFMP and the ¹³CF₃-4-TFMP+O
373 (TP-B-1) (**Table S8**), which suggests that they are ring-opening products of oxidative cleavage.
374 MS² spectra support this (**Figure S12D**), with TP-B-2 showing fragments corresponding to
375 carboxyl group elimination (i.e. loss of CO₂), while MS² of TP-B-3 indicates the presence of
376 hydroxyl and aldehyde groups in the structure. In our experimental setup, no additional oxidants
377 (e.g. H₂O₂) were added, yet a series of oxidation reactions still occurred. This suggests *in situ*
378 photogeneration of ROS via self-sensitized photolysis, a process also observed in the photolysis
379 of tetracycline, fluoroquinolones, and 6PPD.⁶⁰⁻⁶² To test the hypothesis that 4-TFMP undergoes
380 self-sensitized photolysis, photochemical experiments were performed in ultrapure water at
381 three concentrations of 4-TFMP (4, 50, 85 μM). **Figure S13** shows the pseudo-first-order
382 kinetics fitting for the 4-TFMP photolysis in ultrapure water with different initial concentrations,
383 highlighting those higher initial concentrations inhibited photolysis, while lower concentrations
384 enhanced it, indicating that the 4-TFMP photolysis involves self-sensitization mechanism.⁶⁰ As
385 shown in **Figure 4A**, the photolysis rate of 4-TFMP was decreased when the well-known ·OH
386 scavenger methanol (20 mM) was present in the solution, with more reaction suppression at a

387 higher concentration of methanol (80 mM). However, even with methanol in great excess (at
388 20 mM, MeOH:4-TFMP = 400:1), its inhibitory effect on 4-TFMP photolysis was limited.
389 When the methanol concentration was increased to 80 mM (MeOH:4-TFMP = 1600:1), the
390 photodegradation was further suppressed, but the extent of further inhibition was relatively low.
391 Interestingly, the addition of excess FFA (20 mM), a scavenger for $^1\text{O}_2$, inhibited the photolysis
392 of 4-TFMP more effectively than 80 mM methanol (**Figure 4B**). Although FFA also quenches
393 $\cdot\text{OH}$ radicals,^{38,63} the large decrease in photodegradation rate when excessive FFA was present
394 suggests that $^1\text{O}_2$ may play a more prominent role among the generated ROS. $^1\text{O}_2$ has ~20 times
395 longer lifetime in D_2O than in H_2O ,^{40,41} as a $^1\text{O}_2$ enhancer, photodegradation of 4-TFMP was
396 accelerated in 99% D_2O as expected (**Figure 4B**), further demonstrating $^1\text{O}_2$ is a key ROS
397 generated during 4-TFMP photolysis.

398 Based on all evidence presented, we propose that under UV-B irradiation, 4-TFMP
399 undergoes self-sensitized photolysis, wherein 4-TFMP is oxidized, and molecular oxygen
400 either reacts with triplet-state $[4\text{-TFMP}]^*$ to form $^1\text{O}_2$ or is reduced to superoxide. Superoxide
401 is then converted into H_2O_2 , which decomposes to $\cdot\text{OH}$. $\cdot\text{OH}$, a strong oxidant which can attack
402 multiple reactive sites on organic compounds, leading to hydroxylated TPs (i.e. TP-B-1),⁶⁴
403 while $^1\text{O}_2$ is a weaker oxidant which can react with phenols to form hydroperoxides,⁶⁵ leading
404 to ring-opening TPs after hydrolysis (i.e. TP-B-2). As shown in **Figure S14**, $^1\text{O}_2$ can add to the
405 phenol ring through two pathways, forming cyclic peroxides that convert into hydroperoxides.
406 Since the ring-opening product 4-TFMP+2O, formed from the 1,4-addition, does not have
407 characteristic carboxyl group loss in MS^2 , it is likely that the 1,2-addition pathway is favored.
408 TP-B-2 may also form through the reaction of the 4-TFMP radical cation with superoxide, as

409 proposed in a similar mechanism by Deng et al. in lignin photolysis.⁶⁶ Multiple pathways
410 contribute to the formation of TP-B-2, in which the aromatic ring no longer exists, while the –
411 CF₃ group remains, likely corresponding to the -64.50 ppm resonance in the ¹⁹F NMR spectrum.
412 TP-B-2 can undergo further oxidation by various ROS to form TP-B-3, which can then
413 experience deeper oxidative cleavage, eventually yielding TFA. Notably, in a study on bacterial
414 degradation of fluoxetine that produces TFA, the intermediates 4-TFMP+3O were also
415 detected.⁶⁷ Its structure resembles the oxidative ring-opening product 4-TFMP+3O found in
416 photolysis, suggesting similarities in mechanisms between the photolysis of 4-TFMP and its
417 bacterial biotransformation. The oxidative cleavage process of 4-TFMP is analogous to a
418 bleaching process of brown carbon in atmospheric chemistry, where UV-Vis absorbing aromatic
419 compounds are step wise oxidized, resulting in aromatic ring cleavage, the loss of conjugated
420 structures, and a reduction in light absorption.^{68–70}

421 *Pathway C, photodimerization:* Unexpectedly, ¹³CF₃-4-TFMP underwent dimerization
422 during photolysis. While the exact substitution position of the phenoxide could not be
423 determined, the MS² spectrum of the dimer product TP-C-1 clearly indicates that one phenoxide
424 added to the benzene ring of another ¹³CF₃-4-TFMP molecule (**Figure S12F**). Previous studies
425 on phenol oxidation have shown that phenol can polymerize via phenoxide radicals.^{71,72} We
426 hypothesize that the photodimerization of ¹³CF₃-4-TFMP follows a similar mechanism, with
427 self-sensitization still contributing to the process, as the photodimerization of two ¹³CF₃-4-
428 TFMP molecules results in the net formation of one H₂O₂. The dimer product, TP-C-1, contains
429 two –¹³CF₃ groups and further photo-defluorinated through intermediates TP-C-2 and TP-C-3,
430 ultimately forming a ¹³C₂-labeled dimer of 4-HBA (TP-C-4).



432

433 **Figure 4.** Photolysis of 4-TFMP in the presence of excessive (20 mM and 80 mM) methanol (MeOH) as
 434 a $\cdot\text{OH}$ scavenger, in the presence of excessive (20 mM) FFA as a $^1\text{O}_2$ scavenger, and in the presence of
 435 99% D_2O as a $^1\text{O}_2$ enhancer. Note that concentrations measured throughout experiments were normalized
 436 to the initial concentration of 4-TFMP, and the control group is 4-TFMP in ultrapure water without any
 437 additives. Mean and standard deviation of duplicates are shown.

438

439 Environmental Implications

440 Here, we report the kinetics and yields of TFA from aqueous photochemical reactions of 4-
 441 TFMP at different pH, and compare to the yields of TFA from fluoxetine. Currently, TFA is
 442 being reviewed as one of the smallest PFAS across many jurisdictions.^{73,74} In order to
 443 understand the global burden of TFA, production of TFA from aryl- CF_3 compounds must be

444 better characterized. Under our experimental conditions, the yield of TFA from 4-TFMP
445 photolysis ranged from 1.3 to 9.2% depending on the pH of the solution. Fluoxetine had a
446 higher yield than 4-TFMP at alkaline pH, which suggests it may have an additional formation
447 mechanism of TFA – this should be investigated further.

448 Here, we reported the first mechanistic insight including tracking the formation of TFA
449 from 4-TFMP via a series of oxidative additions prior to oxidative cleavage of the aromatic
450 ring. The use of an isotopically-labeled test compound increased confidence of intermediates
451 and TFA formation, which was particularly useful as TFA has notoriously challenging
452 laboratory contamination. There is no doubt that the TFA formed in these experiments
453 originated from 4-TFMP – it did not arise from contamination nor from reactions of an impurity
454 in the experiment.

455 Ideally, reactions of contaminants in the environment will result in complete
456 mineralization, but for 4-TFMP and fluoxetine, they form TFA which persists in the
457 environment and will continue to accumulate if usage continues.⁷⁵ If certain aryl-CF₃ can be
458 designed to undergo defluorination pathways only and not form TFA, we may be able to harness
459 the power of the –CF₃ moiety without producing very persistent TFA.

460 These experiments were performed using lamps centered at UV-B and buffers prepared in
461 the lab. Based on the three proposed pathways, only one forms TFA. It is possible that other
462 oxidative reactions, including indirect photochemistry (which has been observed to form TFA
463 for 4-TFMP²⁷) or microbial reactions,⁶⁷ may increase the yield of TFA compared to what we
464 observed here, thereby increasing the overall contributions of TFA to the environment from 4-
465 TFMP and related compounds. Future studies should investigate the TFA yield from a range of

466 aryl-CF₃ under a range of realistic environmental conditions, including from agrochemicals,
467 since the concentration of TFA in surface waters has been correlated to land use.⁷⁶

468

469 **ACKNOWLEDGEMENTS**

470 Funding for this work was provided by the National Science and Engineering Research Council
471 (NSERC RGPIN-2023-04369 to S.J.) and the Faculty of Science at the University of Alberta.
472 A.A.A. was partially funded by the Lloyd and Margaret Cooley Memorial Studentship in
473 Analytical Chemistry. The authors thank Randy Whittal and Béla Reiz from the University of
474 Alberta Department of Chemistry Mass Spectrometry Facility for assistance with Orbitrap-
475 HRMS and suggestion of isotopic analysis, and thank Liang Li for access to the triple
476 quadrupole MS. The authors also thank Bowen Yang and Geneviève Tremblay (University of
477 Alberta), Alexandra Burnett (McMaster University), and Juliana Laszakovits (ETH Zürich) for
478 their help and discussions.

479

480 **Supporting information**

481 The Supporting Information is available free of charge **online**. A number of references in the
482 **SI** that are not in the main text are cited here.⁷⁷⁻⁸⁰

483

484 **REFERENCES**

485 (1) Hale, S. E.; Neumann, M.; Schliebner, I.; Schulze, J.; Averteck, F. S.; Castell-Exner, C.; Collard,
486 M.; Drmač, D.; Hartmann, J.; Hofman-Caris, R.; Hollender, J.; de Jonge, M.; Kullick, T.;
487 Lennquist, A.; Letzel, T.; Nödler, K.; Pawlowski, S.; Reineke, N.; Rorijs, E.; Scheurer, M.;

- 488 Sigmund, G.; Timmer, H.; Trier, X.; Verbruggen, E.; Arp, H. P. H. Getting in Control of
489 Persistent, Mobile and Toxic (PMT) and Very Persistent and Very Mobile (vPvM) Substances
490 to Protect Water Resources: Strategies from Diverse Perspectives. *Environ. Sci. Eur.* **2022**, *34*
491 (1), 22. <https://doi.org/10.1186/s12302-022-00604-4>.
- 492 (2) Zhai, Z.; Wu, J.; Hu, X.; Li, L.; Guo, J.; Zhang, B.; Hu, J.; Zhang, J. A 17-Fold Increase of
493 Trifluoroacetic Acid in Landscape Waters of Beijing, China during the Last Decade.
494 *Chemosphere* **2015**, *129*, 110–117. <https://doi.org/10.1016/j.chemosphere.2014.09.033>.
- 495 (3) Tian, Y.; Yao, Y.; Chang, S.; Zhao, Z.; Zhao, Y.; Yuan, X.; Wu, F.; Sun, H. Occurrence and Phase
496 Distribution of Neutral and Ionizable Per- and Polyfluoroalkyl Substances (PFASs) in the
497 Atmosphere and Plant Leaves around Landfills: A Case Study in Tianjin, China. *Environ. Sci.*
498 *Technol.* **2018**, *52* (3), 1301–1310. <https://doi.org/10.1021/acs.est.7b05385>.
- 499 (4) Chen, H.; Yao, Y.; Zhao, Z.; Wang, Y.; Wang, Q.; Ren, C.; Wang, B.; Sun, H.; Alder, A. C.;
500 Kannan, K. Multimedia Distribution and Transfer of Per- and Polyfluoroalkyl Substances
501 (PFASs) Surrounding Two Fluorochemical Manufacturing Facilities in Fuxin, China. *Environ.*
502 *Sci. Technol.* **2018**, *52* (15), 8263–8271. <https://doi.org/10.1021/acs.est.8b00544>.
- 503 (5) Cahill, T. M. Increases in Trifluoroacetate Concentrations in Surface Waters over Two Decades.
504 *Environ. Sci. Technol.* **2022**, *56* (13), 9428–9434. <https://doi.org/10.1021/acs.est.2c01826>.
- 505 (6) Freeling, F.; Scheurer, M.; Koschorreck, J.; Hoffmann, G.; Ternes, T. A.; Nödler, K. Levels and
506 Temporal Trends of Trifluoroacetate (TFA) in Archived Plants: Evidence for Increasing
507 Emissions of Gaseous TFA Precursors over the Last Decades. *Environ. Sci. Technol. Lett.* **2022**,
508 *9* (5), 400–405. <https://doi.org/10.1021/acs.estlett.2c00164>.
- 509 (7) Zheng, G.; Eick, S. M.; Salamova, A. Elevated Levels of Ultrashort- and Short-Chain

- 510 Perfluoroalkyl Acids in US Homes and People. *Environ. Sci. Technol.* **2023**, *57* (42), 15782–
511 15793. <https://doi.org/10.1021/acs.est.2c06715>.
- 512 (8) Wang, Z.; Buser, A. M.; Cousins, I. T.; Demattio, S.; Drost, W.; Johansson, O.; Ohno, K.;
513 Patlewicz, G.; Richard, A. M.; Walker, G. W.; White, G. S.; Leinala, E. A New OECD
514 Definition for Per- and Polyfluoroalkyl Substances. *Environ. Sci. Technol.* **2021**, *55* (23),
515 15575–15578. <https://doi.org/10.1021/acs.est.1c06896>.
- 516 (9) OECD. *Reconciling Terminology of the Universe of Per- and Polyfluoroalkyl Substances:*
517 *Recommendations and Practical Guidance*; Organisation for Economic Co-operation and
518 Development: Paris, 2021.
- 519 (10) Pickard, H. M.; Criscitiello, A. S.; Persaud, D.; Spencer, C.; Muir, D. C. G.; Lehnherr, I.; Sharp,
520 M. J.; De Silva, A. O.; Young, C. J. Ice Core Record of Persistent Short-Chain Fluorinated
521 Alkyl Acids: Evidence of the Impact From Global Environmental Regulations. *Geophys. Res.*
522 *Lett.* **2020**, *47* (10), e2020GL087535. <https://doi.org/10.1029/2020GL087535>.
- 523 (11) Rollins, A.; Barber, J.; Elliott, R.; Wood, B. Xenobiotic Monitoring in Plants by ¹⁹F and ¹H
524 Nuclear Magnetic Resonance Imaging and Spectroscopy: Uptake of Trifluoroacetic Acid in
525 *Lycopersicon Esculentum*. *Plant Physiol.* **1989**, *91* (4), 1243–1246.
526 <https://doi.org/10.1104/pp.91.4.1243>.
- 527 (12) Zhang, L.; Sun, H.; Wang, Q.; Chen, H.; Yao, Y.; Zhao, Z.; Alder, A. C. Uptake Mechanisms of
528 Perfluoroalkyl Acids with Different Carbon Chain Lengths (C2–C8) by Wheat (*Triticum*
529 *Aestivum* L.). *Sci. Total Environ.* **2019**, *654*, 19–27.
530 <https://doi.org/10.1016/j.scitotenv.2018.10.443>.
- 531 (13) Scheurer, M.; Nödler, K.; Freeling, F.; Janda, J.; Happel, O.; Riegel, M.; Müller, U.; Storck, F.

- 532 R.; Fleig, M.; Lange, F. T.; Brunsch, A.; Brauch, H.-J. Small, Mobile, Persistent:
533 Trifluoroacetate in the Water Cycle – Overlooked Sources, Pathways, and Consequences for
534 Drinking Water Supply. *Water Res.* **2017**, *126*, 460–471.
535 <https://doi.org/10.1016/j.watres.2017.09.045>.
- 536 (14) Scheringer, M.; Cousins, I. T.; Goldenman, G. Is a Seismic Shift in the Landscape of PFAS
537 Uses Occurring? *Environ. Sci. Technol.* **2024**, *58* (16), 6843–6845.
538 <https://doi.org/10.1021/acs.est.4c01947>.
- 539 (15) Neuwald, I. J.; Hübner, D.; Wiegand, H. L.; Valkov, V.; Borchers, U.; Nödler, K.; Scheurer, M.;
540 Hale, S. E.; Arp, H. P. H.; Zahn, D. Ultra-Short-Chain PFASs in the Sources of German
541 Drinking Water: Prevalent, Overlooked, Difficult to Remove, and Unregulated. *Environ. Sci.*
542 *Technol.* **2022**, *56* (10), 6380–6390. <https://doi.org/10.1021/acs.est.1c07949>.
- 543 (16) Joudan, S.; Silva, A. O. D.; J. Young, C. Insufficient Evidence for the Existence of Natural
544 Trifluoroacetic Acid. *Environ. Sci. Process. Impacts* **2021**, *23* (11), 1641–1649.
545 <https://doi.org/10.1039/D1EM00306B>.
- 546 (17) Kotamarthi, V. R.; Rodriguez, J. M.; Ko, M. K. W.; Tromp, T. K.; Sze, N. D.; Prather, M. J.
547 Trifluoroacetic Acid from Degradation of HCFCs and HFCs: A Three-Dimensional Modeling
548 Study. *J. Geophys. Res. Atmospheres* **1998**, *103* (D5), 5747–5758.
549 <https://doi.org/10.1029/97JD02988>.
- 550 (18) Holland, R.; Khan, M. A. H.; Driscoll, I.; Chhantyal-Pun, R.; Derwent, R. G.; Taatjes, C. A.;
551 Orr-Ewing, A. J.; Percival, C. J.; Shallcross, D. E. Investigation of the Production of
552 Trifluoroacetic Acid from Two Halocarbons, HFC-134a and HFO-1234yf and Its Fates Using
553 a Global Three-Dimensional Chemical Transport Model. *ACS Earth Space Chem.* **2021**, *5* (4),

554 849–857. <https://doi.org/10.1021/acsearthspacechem.0c00355>.

555 (19) Ellis, D. A.; Mabury, S. A.; Martin, J. W.; Muir, D. C. G. Thermolysis of Fluoropolymers as a
556 Potential Source of Halogenated Organic Acids in the Environment. *Nature* **2001**, *412* (6844),
557 321–324. <https://doi.org/10.1038/35085548>.

558 (20) Zhang, Y.; Moores, A.; Liu, J.; Ghoshal, S. New Insights into the Degradation Mechanism of
559 Perfluorooctanoic Acid by Persulfate from Density Functional Theory and Experimental Data.
560 *Environ. Sci. Technol.* **2019**, *53* (15), 8672–8681. <https://doi.org/10.1021/acs.est.9b00797>.

561 (21) Young, C. J.; Mabury, S. A. Atmospheric Perfluorinated Acid Precursors: Chemistry,
562 Occurrence, and Impacts. In *Reviews of Environmental Contamination and Toxicology Volume*
563 *208: Perfluorinated alkylated substances*; De Voogt, P., Ed.; Springer: New York, NY, 2010;
564 pp 1–109. https://doi.org/10.1007/978-1-4419-6880-7_1.

565 (22) Müller, K.; Faeh, C.; Diederich, F. Fluorine in Pharmaceuticals: Looking Beyond Intuition.
566 *Science* **2007**, *317* (5846), 1881–1886. <https://doi.org/10.1126/science.1131943>.

567 (23) Inoue, M.; Sumii, Y.; Shibata, N. Contribution of Organofluorine Compounds to
568 Pharmaceuticals. *ACS Omega* **2020**, *5* (19), 10633–10640.
569 <https://doi.org/10.1021/acsomega.0c00830>.

570 (24) Mole, R. A.; Brooks, B. W. Global Scanning of Selective Serotonin Reuptake Inhibitors:
571 Occurrence, Wastewater Treatment and Hazards in Aquatic Systems. *Environ. Pollut.* **2019**,
572 *250*, 1019–1031. <https://doi.org/10.1016/j.envpol.2019.04.118>.

573 (25) Manfrin, A.; Hänggli, A.; van den Wildenberg, J.; McNeill, K. Substituent Effects on the Direct
574 Photolysis of Benzotrifluoride Derivatives. *Environ. Sci. Technol.* **2020**, *54* (18), 11109–11117.
575 <https://doi.org/10.1021/acs.est.9b07429>.

- 576 (26) Ellis, D. A.; Mabury, S. A. The Aqueous Photolysis of TFM and Related
577 Trifluoromethylphenols. An Alternate Source of Trifluoroacetic Acid in the Environment.
578 *Environ. Sci. Technol.* **2000**, *34* (4), 632–637. <https://doi.org/10.1021/es990422c>.
- 579 (27) Bhat, A. P.; Mundhenke, T. F.; Whiting, Q. T.; Peterson, A. A.; Pomerantz, W. C. K.; Arnold,
580 W. A. Tracking Fluorine during Aqueous Photolysis and Advanced UV Treatment of
581 Fluorinated Phenols and Pharmaceuticals Using a Combined ¹⁹F-NMR, Chromatography, and
582 Mass Spectrometry Approach. *ACS Environ. Au* **2022**, *2* (3), 242–252.
583 <https://doi.org/10.1021/acsenvironau.1c00057>.
- 584 (28) Bhat, A. P.; Pomerantz, W. C. K.; Arnold, W. A. Finding Fluorine: Photoproduct Formation
585 during the Photolysis of Fluorinated Pesticides. *Environ. Sci. Technol.* **2022**, *56* (17), 12336–
586 12346. <https://doi.org/10.1021/acs.est.2c04242>.
- 587 (29) Tisler, S.; Zindler, F.; Freeling, F.; Nödler, K.; Toelgyesi, L.; Braunbeck, T.; Zwiener, C.
588 Transformation Products of Fluoxetine Formed by Photodegradation in Water and
589 Biodegradation in Zebrafish Embryos (*Danio Rerio*). *Environ. Sci. Technol.* **2019**, *53* (13),
590 7400–7409. <https://doi.org/10.1021/acs.est.9b00789>.
- 591 (30) Lam, M. W.; Young, C. J.; Mabury, S. A. Aqueous Photochemical Reaction Kinetics and
592 Transformations of Fluoxetine. *Environ. Sci. Technol.* **2005**, *39* (2), 513–522.
593 <https://doi.org/10.1021/es0494757>.
- 594 (31) Altamura, A. C.; Moro, A. R.; Percudani, M. Clinical Pharmacokinetics of Fluoxetine. *Clin.*
595 *Pharmacokinet.* **1994**, *26* (3), 201–214. <https://doi.org/10.2165/00003088-199426030-00004>.
- 596 (32) Mutlib, A. E. Application of Stable Isotope-Labeled Compounds in Metabolism and in
597 Metabolism-Mediated Toxicity Studies. *Chem. Res. Toxicol.* **2008**, *21* (9), 1672–1689.

598 <https://doi.org/10.1021/tx800139z>.

599 (33) Nelson, T. F.; Baumgartner, R.; Jaggi, M.; Bernasconi, S. M.; Battagliarin, G.; Sinkel, C.;

600 Künkel, A.; Kohler, H.-P. E.; McNeill, K.; Sander, M. Biodegradation of Poly(Butylene

601 Succinate) in Soil Laboratory Incubations Assessed by Stable Carbon Isotope Labelling. *Nat.*

602 *Commun.* **2022**, *13* (1), 5691. <https://doi.org/10.1038/s41467-022-33064-8>.

603 (34) Qian, Y.; Chen, Z.; Wang, J.; Peng, M.; Zhang, S.; Yan, X.; Han, X.; Ou, X.; Sun, J.; Li, S.;

604 Chen, K. H/D Exchange Coupled with 2H-Labeled Stable Isotope-Assisted Metabolomics

605 Discover Transformation Products of Contaminants of Emerging Concern. *Anal. Chem.* **2023**,

606 *95* (33), 12541–12549. <https://doi.org/10.1021/acs.analchem.3c02833>.

607 (35) Zhang, J.; Cao, G.; Wang, W.; Qiao, H.; Chen, Y.; Wang, X.; Wang, F.; Liu, W.; Cai, Z. Stable

608 Isotope-Assisted Mass Spectrometry Reveals *in Vivo* Distribution, Metabolism, and Excretion

609 of Tire Rubber-Derived 6PPD-Quinone in Mice. *Sci. Total Environ.* **2024**, *912*, 169291.

610 <https://doi.org/10.1016/j.scitotenv.2023.169291>.

611 (36) Ben-Tal, Y.; Lloyd-Jones, G. C. Kinetics of a Ni/Ir-Photocatalyzed Coupling of ArBr with RBr:

612 Intermediacy of ArNiII(L)Br and Rate/Selectivity Factors. *J. Am. Chem. Soc.* **2022**, *144* (33),

613 15372–15382. <https://doi.org/10.1021/jacs.2c06831>.

614 (37) Liang, Y.; Taya, A.; Zhao, Z.; Saito, N.; Shibata, N. Deoxyfluorination of Acyl Fluorides to

615 Trifluoromethyl Compounds by FLUOLEAD®/Olah's Reagent under Solvent-Free Conditions.

616 *Beilstein J. Org. Chem.* **2020**, *16* (1), 3052–3058. <https://doi.org/10.3762/bjoc.16.254>.

617 (38) Buxton, G. V.; Greenstock, C. L.; Helman, W. P.; Ross, A. B. Critical Review of Rate Constants

618 for Reactions of Hydrated Electrons, Hydrogen Atoms and Hydroxyl Radicals ($\cdot\text{OH}/\cdot\text{O}^-$ in

619 Aqueous Solution. *J. Phys. Chem. Ref. Data* **1988**, *17* (2), 513–886.

620 <https://doi.org/10.1063/1.555805>.

621 (39) Haag, W. R.; Hoigne, Juerg. Singlet Oxygen in Surface Waters. 3. Photochemical
622 Formation and Steady-State Concentrations in Various Types of Waters. *Environ. Sci. Technol.*
623 **1986**, *20* (4), 341–348. <https://doi.org/10.1021/es00146a005>.

624 (40) Wilkinson, F.; Helman, W. P.; Ross, A. B. Rate Constants for the Decay and Reactions of the
625 Lowest Electronically Excited Singlet State of Molecular Oxygen in Solution. An Expanded
626 and Revised Compilation. *J. Phys. Chem. Ref. Data* **1995**, *24* (2), 663–677.
627 <https://doi.org/10.1063/1.555965>.

628 (41) Ossola, R.; Jönsson, O. M.; Moor, K.; McNeill, K. Singlet Oxygen Quantum Yields in
629 Environmental Waters. *Chem. Rev.* **2021**, *121* (7), 4100–4146.
630 <https://doi.org/10.1021/acs.chemrev.0c00781>.

631 (42) Dulin, David.; Mill, Theodore. Development and Evaluation of Sunlight Actinometers. *Environ.*
632 *Sci. Technol.* **1982**, *16* (11), 815–820. <https://doi.org/10.1021/es00105a017>.

633 (43) Buth, J. M.; Ossola, R.; Partanen, S. B.; McNeill, K.; Arnold, W. A.; O'Connor, M.; Latch, D.
634 E. Kinetics and Pathways of the Aqueous Photolysis of Pharmaceutical Pollutants: A Versatile
635 Laboratory or Remote Learning Investigation. *J. Chem. Educ.* **2021**, *98* (7), 2411–2418.
636 <https://doi.org/10.1021/acs.jchemed.0c01398>.

637 (44) Challis, J. K.; Carlson, J. C.; Friesen, K. J.; Hanson, M. L.; Wong, C. S. Aquatic Photochemistry
638 of the Sulfonamide Antibiotic Sulfapyridine. *J. Photochem. Photobiol. Chem.* **2013**, *262*, 14–
639 21. <https://doi.org/10.1016/j.jphotochem.2013.04.009>.

640 (45) Laszakovits, J. R.; Berg, S. M.; Anderson, B. G.; O'Brien, J. E.; Wammer, K. H.; Sharpless, C.
641 M. P-Nitroanisole/Pyridine and p-Nitroacetophenone/Pyridine Actinometers Revisited:

642 Quantum Yield in Comparison to Ferrioxalate. *Environ. Sci. Technol. Lett.* **2017**, *4* (1), 11–14.
643 <https://doi.org/10.1021/acs.estlett.6b00422>.

644 (46) Anton, L. de B.; Silverman, A. I.; Apell, J. N. Determining Wavelength-Dependent Quantum
645 Yields of Photodegradation: Importance of Experimental Setup and Reference Values for
646 Actinometers. *Environ. Sci. Process. Impacts* **2024**, *26* (6), 1052–1063.
647 <https://doi.org/10.1039/D4EM00084F>.

648 (47) Hoops, S.; Sahle, S.; Gauges, R.; Lee, C.; Pahle, J.; Simus, N.; Singhal, M.; Xu, L.; Mendes,
649 P.; Kummer, U. COPASI—a COmplex PATHway SIMulator. *Bioinformatics* **2006**, *22* (24),
650 3067–3074. <https://doi.org/10.1093/bioinformatics/btl485>.

651 (48) Dearden, J. C.; Weeks, G. R. Relationship of Physicochemical Properties of Isomeric
652 Trifluoromethylphenols with Their Bactericidal Effect on *Escherichia Coli*. *J. Pharm. Sci.* **1973**,
653 *62* (5), 843–844. <https://doi.org/10.1002/jps.2600620540>.

654 (49) Sakai, T. T.; Santi, D. V. Hydrolysis of Hydroxybenzotrifluorides and Fluorinated Uracil
655 Derivatives. General Mechanism for Carbon-Fluorine Bond Labilization. *J. Med. Chem.* **1973**,
656 *16* (10), 1079–1084. <https://doi.org/10.1021/jm00268a003>.

657 (50) Kwon, J.-W.; Armbrust, K. L. Laboratory Persistence and Fate of Fluoxetine in Aquatic
658 Environments. *Environ. Toxicol. Chem.* **2006**, *25* (10), 2561–2568. [https://doi.org/10.1897/05-](https://doi.org/10.1897/05-613R.1)
659 [613R.1](https://doi.org/10.1897/05-613R.1).

660 (51) Bhat, A. P.; Pomerantz, W. C. K.; Arnold, W. A. Fluorinated Pharmaceutical and Pesticide
661 Photolysis: Investigating Reactivity and Identifying Fluorinated Products by Combining
662 Computational Chemistry,¹⁹F NMR, and Mass Spectrometry. *Environ. Sci. Technol.* **2024**, *58*
663 (7), 3437–3448. <https://doi.org/10.1021/acs.est.3c09341>.

- 664 (52) Gauthier, J. R.; Mabury, S. A. Identifying Unknown Fluorine-Containing Compounds in
665 Environmental Samples Using ^{19}F NMR and Spectral Database Matching. *Environ. Sci.*
666 *Technol.* **2023**, *57* (23), 8760–8767. <https://doi.org/10.1021/acs.est.3c01220>.
- 667 (53) Gauthier, J. R.; Mabury, S. A. Noise-Reduced Quantitative Fluorine NMR Spectroscopy
668 Reveals the Presence of Additional Per- and Polyfluorinated Alkyl Substances in
669 Environmental and Biological Samples When Compared with Routine Mass Spectrometry
670 Methods. *Anal. Chem.* **2022**, *94* (7), 3278–3286. <https://doi.org/10.1021/acs.analchem.1c05107>.
- 671 (54) van der Most, M. A.; Bakker, W.; Wesseling, S.; van den Brink, N. W. Toxicokinetics of the
672 Antidepressant Fluoxetine and Its Active Metabolite Norfluoxetine in *Caenorhabditis Elegans*
673 and Their Comparative Potency. *Environ. Sci. Technol.* **2024**, *58* (7), 3129–3140.
674 <https://doi.org/10.1021/acs.est.3c07744>.
- 675 (55) Zindler, F.; Tisler, S.; Loerracher, A.-K.; Zwiener, C.; Braunbeck, T. Norfluoxetine Is the Only
676 Metabolite of Fluoxetine in Zebrafish (*Danio Rerio*) Embryos That Accumulates at
677 Environmentally Relevant Exposure Scenarios. *Environ. Sci. Technol.* **2020**, *54* (7), 4200–4209.
678 <https://doi.org/10.1021/acs.est.9b07618>.
- 679 (56) Joudan, S.; Gauthier, J.; Mabury, S. A.; Young, C. J. Aqueous Leaching of Ultrashort-Chain
680 PFAS from (Fluoro)Polymers: Targeted and Nontargeted Analysis. *Environ. Sci. Technol. Lett.*
681 **2024**, *11* (3), 237–242. <https://doi.org/10.1021/acs.estlett.3c00797>.
- 682 (57) Deng, L.; Zhang, C.; Li, B.; Fu, J.; Zhang, Z.; Li, S.; Zhao, X.; Su, Z.; Hu, C.; Yu, Z. Photo-
683 Induced Defluorination Acyl Fluoride Exchange as a Fluorogenic Photo-Click Reaction for
684 Photo-Affinity Labeling. *Chem. Sci.* **2023**, *14* (13), 3630–3641.
685 <https://doi.org/10.1039/D2SC04636A>.

- 686 (58) Ste-Marie, L.; Boismenu, D.; Vachon, L.; Montgomery, J. Evaluation of Sodium 4-
687 Hydroxybenzoate as an Hydroxyl Radical Trap Using Gas Chromatography–Mass
688 Spectrometry and High-Performance Liquid Chromatography with Electrochemical Detection.
689 *Anal. Biochem.* **1996**, *241* (1), 67–74. <https://doi.org/10.1006/abio.1996.0379>.
- 690 (59) Freinbichler, W.; Bianchi, L.; Colivicchi, M. A.; Ballini, C.; Tipton, K. F.; Linert, W.; Corte, L.
691 D. The Detection of Hydroxyl Radicals *in Vivo*. *J. Inorg. Biochem.* **2008**, *102* (5), 1329–1333.
692 <https://doi.org/10.1016/j.jinorgbio.2007.12.017>.
- 693 (60) Werner, J. J.; Arnold, W. A.; McNeill, K. Water Hardness as a Photochemical Parameter:
694 Tetracycline Photolysis as a Function of Calcium Concentration, Magnesium Concentration,
695 and pH. *Environ. Sci. Technol.* **2006**, *40* (23), 7236–7241. <https://doi.org/10.1021/es060337m>.
- 696 (61) Huang, S.; Zhang, Z.; Lin, C.; Cheng, H. Solar Photodegradation of a Novel Des-F(6)-
697 Fluoroquinolone, Garenoxacin, and Ecotoxicity of Its Phototransformation Products. *Environ.*
698 *Sci. Technol.* **2024**, *58* (31), 13918–13928. <https://doi.org/10.1021/acs.est.4c03206>.
- 699 (62) Zhou, Y.; Yixi, L.; Kong, Q.; Peng, J.; Pan, Y.; Qiu, J.; Yang, X. Sunlight-Induced
700 Transformation of Tire Rubber Antioxidant N-(1,3-Dimethylbutyl)-N'-Phenyl-p-
701 Phenylenediamine (6PPD) to 6PPD-Quinone in Water. *Environ. Sci. Technol. Lett.* **2023**, *10* (9),
702 798–803. <https://doi.org/10.1021/acs.estlett.3c00499>.
- 703 (63) Hu, X.; Zhu, M. Were Persulfate-Based Advanced Oxidation Processes Really Understood?
704 Basic Concepts, Cognitive Biases, and Experimental Details. *Environ. Sci. Technol.* **2024**, *58*
705 (24), 10415–10444. <https://doi.org/10.1021/acs.est.3c10898>.
- 706 (64) Gligorovski, S.; Streckowski, R.; Barbati, S.; Vione, D. Environmental Implications of Hydroxyl
707 Radicals ($\bullet\text{OH}$). *Chem. Rev.* **2015**, *115* (24), 13051–13092. <https://doi.org/10.1021/cr500310b>.

- 708 (65) Ghogare, A. A.; Greer, A. Using Singlet Oxygen to Synthesize Natural Products and Drugs.
709 *Chem. Rev.* **2016**, *116* (17), 9994–10034. <https://doi.org/10.1021/acs.chemrev.5b00726>.
- 710 (66) Deng, Y.; Zhu, K.; Jiang, W.; Liu, Y.; Xie, L.; Liu, F.; Yang, K.; Jiang, Y.; Jia, H. Novel Chemical
711 Routes for Carbon Dioxide and Methane Production from Lignin Photodegradation: The Role
712 of Environmental Free Radicals. *Environ. Sci. Technol.* **2024**.
713 <https://doi.org/10.1021/acs.est.4c03414>.
- 714 (67) Khan, M. F.; Murphy, C. D. Bacterial Degradation of the Anti-Depressant Drug Fluoxetine
715 Produces Trifluoroacetic Acid and Fluoride Ion. *Appl. Microbiol. Biotechnol.* **2021**, *105* (24),
716 9359–9369. <https://doi.org/10.1007/s00253-021-11675-3>.
- 717 (68) Hems, R. F.; Abbatt, J. P. D. Aqueous Phase Photo-Oxidation of Brown Carbon Nitrophenols:
718 Reaction Kinetics, Mechanism, and Evolution of Light Absorption. *ACS Earth Space Chem.*
719 **2018**, *2* (3), 225–234. <https://doi.org/10.1021/acsearthspacechem.7b00123>.
- 720 (69) Laskin, A.; Laskin, J.; Nizkorodov, S. A. Chemistry of Atmospheric Brown Carbon. *Chem. Rev.*
721 **2015**, *115* (10), 4335–4382. <https://doi.org/10.1021/cr5006167>.
- 722 (70) Zhao, R.; Lee, A. K. Y.; Huang, L.; Li, X.; Yang, F.; Abbatt, J. P. D. Photochemical Processing
723 of Aqueous Atmospheric Brown Carbon. *Atmospheric Chem. Phys.* **2015**, *15* (11), 6087–6100.
724 <https://doi.org/10.5194/acp-15-6087-2015>.
- 725 (71) Peng, J.; Zhou, P.; Zhou, H.; Huang, B.; Sun, M.; He, C.-S.; Zhang, H.; Ao, Z.; Liu, W.; Lai, B.
726 Removal of Phenols by Highly Active Periodate on Carbon Nanotubes: A Mechanistic
727 Investigation. *Environ. Sci. Technol.* **2023**, *57* (29), 10804–10815.
728 <https://doi.org/10.1021/acs.est.2c08266>.
- 729 (72) Chen, Y.; Ren, W.; Ma, T.; Ren, N.; Wang, S.; Duan, X. Transformative Removal of Aqueous

730 Micropollutants into Polymeric Products by Advanced Oxidation Processes. *Environ. Sci.*
731 *Technol.* **2024**, 58 (11), 4844–4851. <https://doi.org/10.1021/acs.est.3c06376>.

732 (73) Canada, E. and C. C. *Updated draft state of per- and polyfluoroalkyl substances (PFAS) report.*
733 [https://www.canada.ca/en/environment-climate-change/services/evaluating-existing-](https://www.canada.ca/en/environment-climate-change/services/evaluating-existing-substances/updated-draft-state-per-polyfluoroalkyl-substances-report.html)
734 [substances/updated-draft-state-per-polyfluoroalkyl-substances-report.html](https://www.canada.ca/en/environment-climate-change/services/evaluating-existing-substances/updated-draft-state-per-polyfluoroalkyl-substances-report.html) (accessed 2024-09-
735 18).

736 (74) *Registry of CLH intentions until outcome - ECHA.* [https://echa.europa.eu/de/registry-of-clh-](https://echa.europa.eu/de/registry-of-clh-intentions-until-outcome/-/dislist/details/0b0236e188e6e587)
737 [intentions-until-outcome/-/dislist/details/0b0236e188e6e587](https://echa.europa.eu/de/registry-of-clh-intentions-until-outcome/-/dislist/details/0b0236e188e6e587) (accessed 2024-09-18).

738 (75) T. Cousins, I.; C. DeWitt, J.; Glüge, J.; Goldenman, G.; Herzke, D.; Lohmann, R.; A. Ng, C.;
739 Scheringer, M.; Wang, Z. The High Persistence of PFAS Is Sufficient for Their Management as
740 a Chemical Class. *Environ. Sci. Process. Impacts* **2020**, 22 (12), 2307–2312.
741 <https://doi.org/10.1039/D0EM00355G>.

742 (76) Cahill, T. M. Assessment of Potential Accumulation of Trifluoroacetate in Terminal Lakes.
743 *Environ. Sci. Technol.* **2024**, 58 (6), 2966–2972. <https://doi.org/10.1021/acs.est.3c08822>.

744 (77) Still, W. C.; Kahn, M.; Mitra, A. Rapid Chromatographic Technique for Preparative Separations
745 with Moderate Resolution. *J. Org. Chem.* **1978**, 43 (14), 2923–2925.
746 <https://doi.org/10.1021/jo00408a041>.

747 (78) Wang, X.; Xu, Y.; Mo, F.; Ji, G.; Qiu, D.; Feng, J.; Ye, Y.; Zhang, S.; Zhang, Y.; Wang, J. Silver-
748 Mediated Trifluoromethylation of Aryldiazonium Salts: Conversion of Amino Group into
749 Trifluoromethyl Group. *J. Am. Chem. Soc.* **2013**, 135 (28), 10330–10333.
750 <https://doi.org/10.1021/ja4056239>.

751 (79) Zhu, D.-L.; Li, J.; Wu, Q.; Wang, Y.; Young, D. J.; Li, H.-X. Room-Temperature, Transition-

752 Metal-Free Arylation of Alcohols with Aryl Bromides. *Synthesis* **2022**, *55*, 637–646.

753 <https://doi.org/10.1055/a-1932-6146>.

754 (80) Schymanski, E. L.; Jeon, J.; Gulde, R.; Fenner, K.; Ruff, M.; Singer, H. P.; Hollender, J.

755 Identifying Small Molecules via High Resolution Mass Spectrometry: Communicating

756 Confidence. *Environ. Sci. Technol.* **2014**, *48* (4), 2097–2098.

757 <https://doi.org/10.1021/es5002105>.

758